UNSTEADY BOUNDARY LAYER FLOW AND HEAT TRANSFER OF OLDROYD-B NANOFLUID TOWARDS A STRETCHING SHEET WITH VARIABLE THERMAL CONDUCTIVITY

by

Sandile Sydney MOTSA* and Mohammad Sharifuddin ANSARI

School of Mathematics, Statistics and Computer Science, University of KwaZulu-Natal, Scottsville, Pietermaritzburg, South Africa

Original scientific paper
DOI: 10.2298/TSCI15S1S39M

This paper presents a time dependent boundary layer flow and heat transfer of an incompressible Oldroyd-B nanofluid past an impulsively stretching sheet. Heat transfer analysis is carried out by taking thermal conductivity as a function of temperature. The non-dimensionalized partial differential equations are solved using bivariate spectral quasi-linearization method). The employs the concept of quasi-linearization to obtain a linear system of partial differential equations which is subsequently solved using a spectral collocation method that uses bivariate Lagrange interpolating polynomials as basic functions. This method is found to converge rapidly and is very effective in yielding accurate results. Numerical results have been presented graphically to illustrate the details of flow and heat transfer characteristics and their dependence on some of the physical parameters.

Key words: *variable thermal conductivity, nanofluid, Oldroyd B fluid, impulsive stretching sheet, bivariate spectral quasi-linearization method*

Introduction

Enhancement of heat transfer performance in many industrial and engineering fields such as power, manufacturing, and transportation, is an essential topic from an energy saving perspective. The low thermal conductivity of conventional heat transfer fluids such as water, oils, ethylene glycol, bio-fluids, polymer solutions and some lubricants, is a primary limitation in enhancing the performance and the compactness of such systems. Solids typically have a higher thermal conductivity than liquids. For example, copper has a thermal conductivity that is 700 times greater than that of water and 3000 times greater than that of engine oil. Enhancing heat transfer using solid particles of size up to 100 nm [1, 2] in the base fluid, *i. e.* nanofluids (NF), is an innovative technique. A non-homogeneous equilibrium model proposed by Buongiorno [3] revealed that such a massive increase in the thermal conductivity occurs due to the presence of two main effects, namely the Brownian diffusion and thermophoretic diffusion of nano-scale particles. Nadeem *et al.* [4] carried out a numerical investigation on the steady flow of a Jeffrey fluid model in the presence of nanoparticles (NP) over a linear stretching sheet. The effects of elasticity, Brownian motion, and thermophoresis on the flow of Oldroyd-B NF past a linearly stretching sheet were reported by Nadeem *et al.* [5].

* Corresponding author; e-mail: sandilemotsa@gmail.com

Uddin *et al.* [6] studied the two-dimensional magnetohydrodynamic boundary layer flow of non-Newtonian power-law nanofluid past a linearly stretching sheet with linear hydrodynamic slip boundary conditions. Recently Khan *et al.* [7] obtained series solutions of steady three dimensional boundary layer flow of an Oldroyd-B fluid over a bidirectional stretching surface with heat generation/absorption effects. All the above mentioned studies deal with steady NF flows over stretching sheets. Unsteady NF flows due to stretching sheet have received less attention. A few of such studies have been considered by Bachok *et al.* [8], Khan *et al.*[9], Mustafa *et al.* [10], and Beg *et al.* [11].

The objective of the present study is to investigate the dynamics of boundary layer flow of an Oldroyd-B nanofluid with variable thermal conductivity considering Buongiorno's [3] model over an impulsively stretched sheet. It is assumed that the temperature and concentration of the sheet are suddenly raised from that of the surrounding fluid. The Oldroyd-B fluid model is one which takes into account the effect of relaxation and retardation time [12-17]. The variable thermal conductivity is quite common in polyme (where $a > 0$ is a constant), temperature T_w, and NP concentration C_w. The x- and y- axis are taken along and perpendicular to the sheet, respectively. It is assumed that both the fluid phase and NP are in thermal equilibrium state. The fluid properties are assumed to be constant, except for the fluid thermal conductivity which is taken as a linear function of temperature.

The boundary layer equations of Oldroyd-B fluid model along with the thermal energy and NP concentration are [5]:

$$\frac{\partial u}{\partial x}+\frac{\partial v}{\partial y}=0 \tag{1a}$$

$$\frac{\partial u}{\partial t}+u\frac{\partial u}{\partial x}+v\frac{\partial u}{\partial y}+K_1\left[u^2\frac{\partial^2 u}{\partial x^2}+v^2\frac{\partial^2 v}{\partial y^2}+2uv\frac{\partial^2 u}{\partial x\partial y}\right]=$$
$$=\nu\frac{\partial^2 u}{\partial y^2}+\nu K_2\left\{u\frac{\partial^3 u}{\partial x\partial y^2}+v\frac{\partial^3 u}{\partial y^3}-\frac{\partial u}{\partial x}\frac{\partial^2 u}{\partial y^2}-\frac{\partial u}{\partial y}\frac{\partial^2 v}{\partial y^2}\right\} \tag{1b}$$

$$(\rho c)_f\left(\frac{\partial T}{\partial t}+u\frac{\partial T}{\partial x}+v\frac{\partial T}{\partial y}\right)=\frac{\partial}{\partial y}\left(k\frac{\partial T}{\partial y}\right)+(\rho c)_p\left[D_B\frac{\partial C}{\partial y}\frac{\partial T}{\partial y}+\frac{D_T}{T_\infty}\left(\frac{\partial T}{\partial y}\right)^2\right] \tag{1c}$$

$$\frac{\partial C}{\partial t}+u\frac{\partial C}{\partial x}+v\frac{\partial C}{\partial y}=\frac{\partial}{\partial y}\left(k\frac{\partial T}{\partial y}\right)+(\rho c)_p\left[D_B\frac{\partial C}{\partial y}\frac{\partial T}{\partial y}+\frac{D_T}{T_\infty}\left(\frac{\partial T}{\partial y}\right)^2\right] \tag{1d}$$

The associated boundary conditions are:

$$\begin{cases} t\geq 0, \quad y=0:\ u=U_w(x)=ax, \quad v=0, \quad T=T_w, \quad C=C_w \\ t\geq 0, \quad y\to\infty:\ u\to 0, \quad \dfrac{\partial u}{\partial x}\to 0, \quad T=T_\infty, \quad C=C_\infty \end{cases} \tag{2a, b}$$

The fluid thermal conductivity is assumed to vary as a linear function of the temperature in the form:

$$k = k_\infty[1 + b(T - T_\infty)] \tag{3}$$

Equations (1a, b, c, d) can be transformed into equivalent partial differential equations using the similarity solution technique. To achieve this, we introduce the following similarity variables ξ and η:

$$\eta = y\sqrt{\frac{a}{\upsilon\xi}}, \quad \xi = 1 - \mathrm{e}^{-\tau}, \quad \tau = at, \quad \psi = x\sqrt{a\upsilon\xi}\, f(\xi,\eta)$$
$$\theta(\xi,\eta) = \frac{T - T_\infty}{T_w - T_\infty}, \quad \phi(\xi,\eta) = \frac{C - C_\infty}{C_w - C_\infty} \tag{4a, b, c, d, e, f}$$

where $f(\xi,\eta)$ is the dimensionless stream function. The velocity components are related to the stream function as $u = \partial\psi/\partial y$ and $v = -\partial\psi/\partial x$.

Substituting ψ, θ, and ϕ into eqs. (1a, b, c, d), the equivalent partial differential equations governing the flow are obtained as:

$$f''' + 0.5\eta(1-\xi)f'' + \beta_2\{ff'''' - (f'')^2\} - \xi\{(f')^2 - ff''\} =$$
$$= \beta_1\xi\{f^2 f''' - 2ff'f''\} + \xi(1-\xi)\frac{\partial f'}{\partial\xi} \tag{5}$$

$$\frac{1}{\mathrm{Pr}}[(1+S\theta)\theta'' + S(\theta')^2] + \xi f\theta' + Nb\phi'\theta' + Nt(\theta')^2 = (1-\xi)\left(\xi\frac{\partial\theta}{\partial\xi} - \frac{\eta}{2}\theta'\right) \tag{6}$$

$$\phi'' + \mathrm{Le}\,\xi f\phi' + \mathrm{Le}(1-\xi)\left\{\frac{\eta}{2}\phi' - \xi\frac{\partial\phi}{\partial\xi}\right\} + \frac{Nt}{Nb}\theta'' = 0 \tag{7}$$

and the associated boundary conditions become:

$$f'(0,\xi) = 1, \quad f(0,\xi) = 0, \quad \theta(0,\xi) = 1, \quad \phi(0,\xi) = 1 \tag{8a, b, c, d}$$

where

$$Nt = (\rho c)_p D_T \frac{T_w - T_\infty}{\upsilon T_\infty (\rho c)_f}, \quad \beta_1 = aK_1, \quad \beta_2 = aK_2, \quad \mathrm{Le} = \frac{\upsilon}{D_B}, \quad \mathrm{Pr} = \frac{\upsilon}{a},$$
$$S = b(T_w - T_\infty), \quad Nb = (\rho c)_p D_B \frac{T_w - T_\infty}{\upsilon(\rho c)_f}$$

The local Nusselt number Nu_x and the local Sherwood number Sh_x are defined as:

$$\mathrm{Nu}_x\,\mathrm{Re}_x^{-1/2}\,\xi^{-1/2} = -\left.\frac{\partial\theta}{\partial\eta}\right|_{\eta=0}, \qquad \mathrm{Sh}_x\,\mathrm{Re}_x^{-1/2}\,\xi^{-1/2} = -\left.\frac{\partial\phi}{\partial\eta}\right|_{\eta=0} \tag{9a,b}$$

where $\mathrm{Re}_x = U_w(x)x/\upsilon$ is the local Reynolds number.

Solution procedure

In view of the dependence on $f(\eta, \xi)$ only, the momentum eq. (5) is solved independently of eqs. (6) and (7) which are, in turn, solved simultaneously for $\theta(\eta, \xi)$, and $\phi(\eta, \xi)$. The quasi-linearisation method is employed to linearise the equations before they are solved iteratively using the Chebyshev spectral collocation method.

Applying the quasi-linearisation procedure on eqs.(5)-(7), we give:

$$a_{0,r}(\eta, \xi) f_{r+1}''' + a_{1,r}(\eta, \xi) f_{r+1}''' + a_{2,r}(\eta, \xi) f_{r+1}'' + a_{3,r}(\eta, \xi) f_{r+1}' + \\ + a_{4,r}(\eta, \xi) f_{r+1} - \xi(1-\xi)\frac{\partial f_{r+1}'}{\partial \xi} = a_{5,r}(\eta, \xi) \tag{10}$$

$$b_{0,r}(\eta, \xi)\theta_{r+1}'' + b_{1,r}(\eta, \xi)\theta_{r+1}' + b_{2,r}(\eta, \xi)\theta_{r+1} + b_{3,r}(\eta, \xi)\phi_{r+1}' - \xi(1-\xi)\frac{\partial \theta_{r+1}}{\partial \xi} = b_{4,r}(\eta, \xi) \tag{11}$$

$$\phi_{r+1}'' + c_{1,r}(\eta, \xi)\phi_{r+1}' + \frac{Nt}{Nb}\theta_{r+1}'' - \mathrm{Le}\xi(1-\xi)\frac{\partial \phi_{r+1}}{\partial \xi} = 0 \tag{12}$$

where

$$a_{0,r}(\eta, \xi) = \beta_2 f_r, \qquad a_{1,r}(\eta, \xi) = 1 - \xi\beta_1 f_r{}^2 \tag{13a, b}$$

$$a_{2,r}(\eta, \xi) = \frac{\eta}{2}(1-\xi) + \xi f_r + 2\xi\beta_1 f_r f_r' - 2\beta_2 f_r'' \\ a_{3,r}(\eta, \xi) = -2\xi f_r' + 2\xi\beta_1 f_r f_r'' \tag{13c, d}$$

$$a_{4,r}(\eta, \xi) = \xi f_r'' + 2\xi\beta_1 f_r' f_r'' - 2\xi\beta_1 f_r f_r''' + \beta_2 f_r'''' \tag{13e}$$

$$a_{5,r}(\eta, \xi) = \xi[f_r f_r'' - (f_r')^2 + 2\beta_1(2 f_r f_r' f_r'' - f_r{}^2 f_r''')] + \beta_2(f_r f_r'''' - f_r''^2) \tag{13f}$$

$$b_{0,r}(\eta, \xi) = \frac{1}{\mathrm{Pr}}(1 + S\theta_r), \quad b_{1,r}(\eta, \xi) = \frac{\eta}{2}(1-\xi) + \xi f_{r+1} + Nb\phi_r' + 2\left(Nt + \frac{S}{\mathrm{Pr}}\right)\theta_r' \tag{13g, h}$$

$$b_{2,r}(\eta, \xi) = \frac{S}{\mathrm{Pr}}\theta_r'', \qquad b_{3,r}(\eta, \xi) = Nb\theta_r', \\ b_{4,r}(\eta, \xi) = Nb\phi_r'\theta_r' + \left(Nt + \frac{S}{\mathrm{Pr}}\right)(\theta_r')^2 + \frac{S}{\mathrm{Pr}}\theta_r\theta_r'' \tag{13j, k, l}$$

$$c_{1,r}(\eta, \xi) = \mathrm{Le}\xi f_r + \frac{\eta}{2}\mathrm{Le}(1-\xi) \tag{13m}$$

The boundary conditions remain the same as eqs. (8a, b, c, d) but are evaluated at the current iteration (denoted with subscript $r+1$).

We apply the Chebyshev spectral collocation method that uses bivariate Lagrange interpolation polynomials as basic functions and the so-called Gauss-Lobatto collocation points as interpolation nodes. To this end, we define the following approximating functions:

$$f(\eta,\xi)\approx\sum_{i=0}^{N_\eta}\sum_{j=0}^{N_\xi}f(\tau_i,\zeta_j)L_i(\tau)L_j(\zeta) \tag{14a}$$

$$\theta(\eta,\xi)\approx\sum_{i=0}^{N_\eta}\sum_{j=0}^{N_\xi}\theta(\tau_i,\zeta_j)L_i(\tau)L_j(\zeta) \tag{14b}$$

$$\phi(\eta,\xi)\approx\sum_{i=0}^{N_\eta}\sum_{j=0}^{N_\xi}\phi(\tau_i,\zeta_j)L_i(\tau)L_j(\zeta) \tag{14c}$$

where L_i and L_j are the standard Lagrange interpolation polynomials defined on the collocation points:

$$\tau_i=\cos\frac{i\pi}{N_\eta},\quad \zeta_i=\cos\frac{j\pi}{N_\xi} \tag{15a, b}$$

for $i=0,1,...,N_\eta$, and $j=0,1,2,...,N_\xi$. Linear transformations are used to transform η and ξ onto the intervals $[-1,1]$ on which the Gauss-Lobatto grid points are defined. With the definitions (14a, b, c) and (15a, b) the continuous derivatives in η and ξ can be approximated at the collocations points in terms of the Chebyshev differentiation matrices [18] as:

$$\left.\frac{\partial^p f_{r+1}}{\partial\eta^p}\right|_{\eta=\eta_j}=\left(\frac{2}{\eta_e}\right)^p\sum_{k=0}^{N_\eta}\mathrm{D}^p{}_{j,k}F_{r+1}(\tau_k,\zeta_i)=\boldsymbol{D}^{\boldsymbol{p}}\boldsymbol{F}_{r+1,i} \tag{16}$$

where p is the order of the derivative, η_e is a finite value chosen to be large enough to approximate the conditions at infinity, $\boldsymbol{D}=(2/\eta_e)[D_{j,k}](j,k=0,1,2,...,N_\eta)$ with $[D_{j,k}]$ being an $(N_\eta+1)$ x $(N_\eta+1)$ Chebyshev derivative matrix, and the vector $\boldsymbol{F}_{r+1,i}$ is defined by:

$$\boldsymbol{F}_{r+1,i}=[F_{r+1,i}(\tau_0),F_{r+1,i}(\tau_1),...,F_{r+1,i}(\tau_{N_\eta})],\quad F_{r+1,i}(\tau_k)=F_{r+1}(\tau_k,\zeta_i) \tag{17a, b}$$

Similarly, the derivative in ξ is approximated at the collocation points in ζ as:

$$\left.\frac{\partial f_{r+1}}{\partial\xi}\right|_{\xi=\xi_i}=2\sum_{k=0}^{N_\xi}\mathrm{d}_{i,k}\,f_{r+1}(\tau,\zeta_k) \tag{18}$$

where $\mathrm{d}_{i,k}$ is the Chebyshev differentiation matrix that has been evaluated separately for the ξ direction.

Applying spectral collocation on eq. (12) gives:

$$\boldsymbol{A}^{(i)}\boldsymbol{F}_{r+1,i}-2\xi_i(1-\xi_i)\sum_{j=0}^{N_\xi}d_{i,j}\boldsymbol{D}\boldsymbol{F}_{r+1,j}=\boldsymbol{R}_1{}^{(i)} \tag{19}$$

where $\boldsymbol{A}^{(i)}=\boldsymbol{a}_{0,r}{}^{(i)}\boldsymbol{D}^4+\boldsymbol{a}_{1,r}{}^{(i)}\boldsymbol{D}^3+\boldsymbol{a}_{2,r}{}^{(i)}\boldsymbol{D}^2+\boldsymbol{a}_{3,r}{}^{(i)}\boldsymbol{D}+\boldsymbol{a}_{4,r}{}^{(i)}$, $\boldsymbol{R}_1^{(i)}=\boldsymbol{a}_{5,r}{}^{(i)}$ with $\boldsymbol{a}_{k,r}{}^{(i)}=a_{k,r}(\eta,\xi_i)$.

The boundary conditions are imposed on eq. (19) for each $i=0,1,...,N_\xi$. In view of the application of bivariate interpolation, spectral collocation and quasi-linearization, the approximation method is termed as the bivariate spectral quasi-linearization method (BSQLM). The BSQLM can be applied in eqs. (11) and (12) to give:

$$\boldsymbol{B}_1^{(i)}\vec{\Theta}_{r+1,i} + \boldsymbol{B}_2^{(i)}\vec{\Phi}_{r+1,i} - 2\xi_i(1-\xi_i)\sum_{j=0}^{N_\xi} \mathrm{d}_{i,j}\vec{\Theta}_{r+1,j} = \boldsymbol{R}_2^{(i)} \tag{20}$$

$$\boldsymbol{B}_3^{(i)}\vec{\Theta}_{r+1,i} + \boldsymbol{B}_4^{(i)}\vec{\Phi}_{r+1,i} - 2\mathrm{Le}\xi_i(1-\xi_i)\sum_{j=0}^{N_\xi} \mathrm{d}_{i,j}\vec{\Phi}_{r+1,j} = \boldsymbol{R}_3^{(i)} \tag{21}$$

where
$\boldsymbol{B}_1^{(i)} = b_{0,r}^{(i)}\boldsymbol{D}^2 + b_{1,r}^{(i)}\boldsymbol{D} + b_{2,r}^{(i)}$, $\boldsymbol{B}_2^{(i)} = b_{3,r}^{(i)}\boldsymbol{D}$, $\boldsymbol{B}_4^{(i)} = \boldsymbol{D}^2 + c_{1,r}^{(i)}\boldsymbol{D}$, $\boldsymbol{B}_2^{(i)} = (Nt/Nb)\boldsymbol{D}^2$,
$\boldsymbol{R}_2^{(i)} = b_{4,r}^{(i)}$, $\boldsymbol{R}_3^{(i)} = \boldsymbol{O}_1$, and $\mathbf{O}_1$ is an $(N_n + 1)\times 1$ vector of zeros. The vectors $\vec{\Theta}_{r+1,i}$ and $\vec{\Phi}_{r+1,i}$ denote the values of θ and ϕ approximated at the collocation points. eqs- (19)-(21) can be written as a matrix system of equations that can be solved iteratively to give the approximate solutions for $f(\eta, \xi)$, $\theta(\eta, \xi)$, and $\phi(\eta, \xi)$.

Results and discussions

The bivariate spectral quasi-linearization method described in the previous section was used to solve the governing partial differential equations to give approximate results for velocity, temperature, concentration, skin friction, heat and mass transfer rates at the wall. In this section we present the results for the important physical properties of the flow for the various input parameters. Unless otherwise specified, the number of collocation points used to generate results was $N_\eta = 60$ and $N_\xi = 10$. Grid independence tests revealed that these choice of collocation points in the η and ξ domains, respectively, were sufficient to give accurate results. The accuracy of the computed results was assessed by measuring the solution based error which is defined as the difference between the approximate solution at the current and previous iteration levels, denoted by the subscripts $r+1$ and r, respectively. The norms of solution based errors were used to measure the convergence of the solution algorithm over a number of iterations. The following error norms are defined for the difference between approximate values of f, θ, and ϕ at successive iterations:

$$E_f = \max_{0\le i\le N_\xi} \left\| F_{r+1,i} - F_{r,i} \right\|_\infty, \quad E_\theta = \max_{0\le i\le N_\xi} \left\| \vec{\Theta}_{r+1,i} - \vec{\Theta}_{r,i} \right\|_\infty, \quad E_\phi = \max_{0\le i\le N_\xi} \left\| \vec{\Phi}_{r+1,i} - \vec{\Phi}_{r,i} \right\|_\infty \tag{22}$$

The variations of E_f, E_θ, and E_ϕ with iterations are shown in fig. 1 when $N_\xi = 10$, $N_\eta = 30$, $\beta_1 = \beta_2 = 0.1$, $Nt = 0.1$, $Nb = 0.1$, $\mathrm{Le} = 10$, $\mathrm{Pr} = 10$. Plots of temperature $\theta(\eta, \xi)$ and NP concentration $\phi(\eta, \xi)$ for different values of thermal conductivity parameter S are displayed in figs. 2 and 3, when Pr = 6.2, $Nt = Nb = 0.1$, $\mathrm{Le} = 5$, $\beta_1 = \beta_2 = 0.1$, and $\xi = 0.75$.

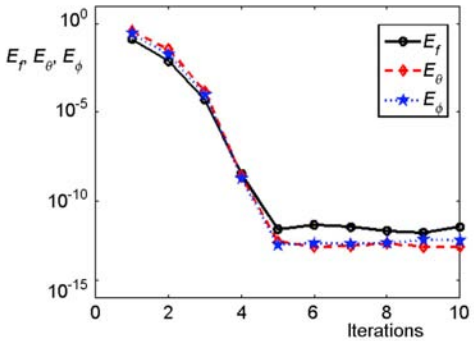

Figure 1. Solution error norms against iterations

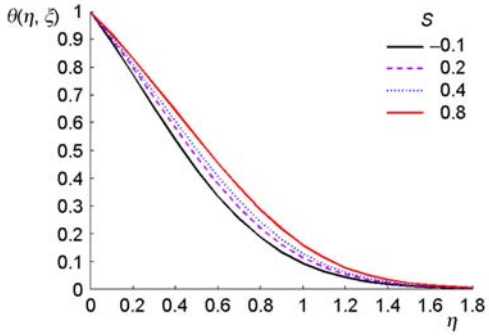

Figure 2. Temperature profiles for different *S*

Figures 4 and 5 are organized to reveal the effect of β_1 on the temperature and concentration profiles when Pr = 6.2, $Nt = Nb = 0.1$, $\mathrm{Le} = 5$, $S = 0.2$, $\beta_2 = 0.1$, and ξ = 0.75. Figure 6 shows the variation in θ profiles for different β_2. It can be seen from the figure that increasing β_2 results in a marginal reduction in the temperature of the fluid within the boundary layer. Temperature profiles for different values of Nt are plotted in fig. 7 when Pr = 6.2, $\mathrm{Le} = 5$, $S = 0.2$, $\beta_1 = \beta_2 = 0.1$, $Nb = 0.1$, and $\xi = 0.75$. Figures 8 and 9 exhibit the impact of dimensionless time ξ on the temperature and concentration profiles within the boundary layer region when Pr = 6.2, $Nt = Nb = 0.1$, $\mathrm{Le} = 5$, $\beta_1 = \beta_2 = 0.1$, and $S = 0.2$. Combined behav-

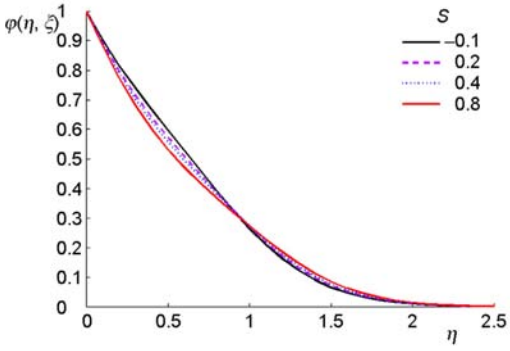

Figure 3. Concentration profiles for different *S*

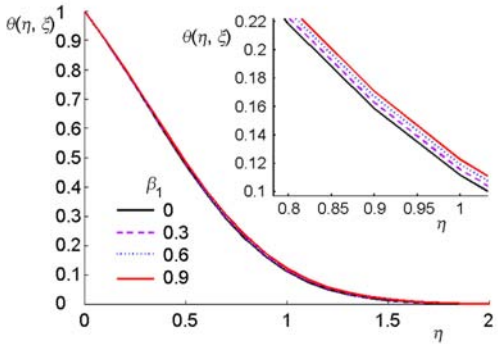

Figure 4. Variations in θ profiles for different β_1

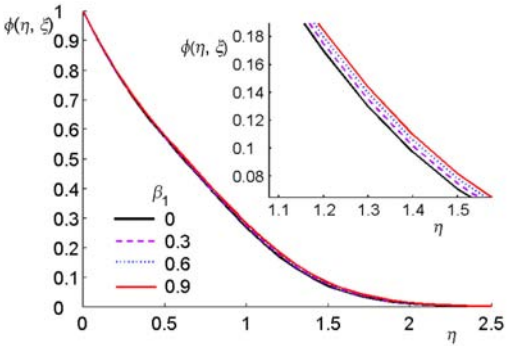

Figure 5. Variations in ϕ profiles for different β_1

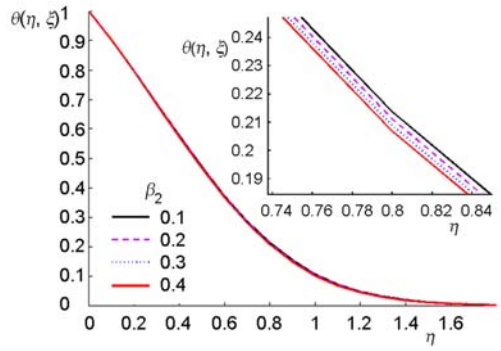

Figure 6. Variations in θ profiles for different β_2

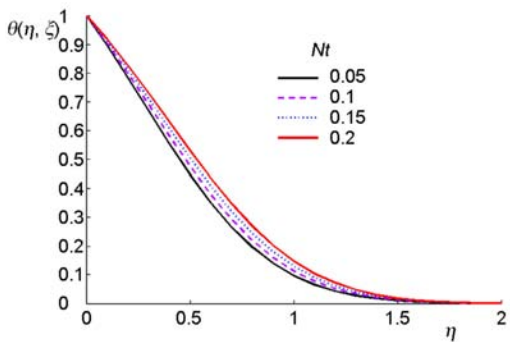

Figure 7. Influence of *Nt* on θ distribution

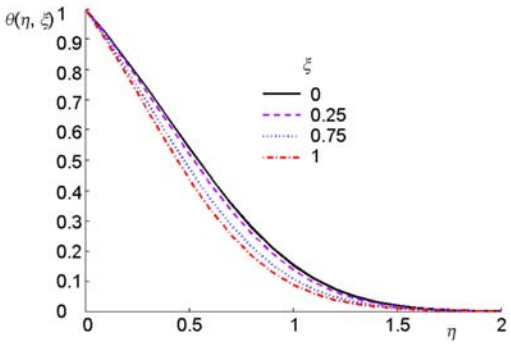

Figure 8. Variations in θ profiles for different ξ

iors of S and ξ on reduced Nusselt number are sketched in fig. 10 when Pr = 6.2, $Nb = Nt = 0.1$, $\beta_1 = \beta_2 = 0.1$, and $\mathrm{Le} = 5$. Figures 11 and 12 are drawn to reveal the impact of β_1 and β_2 on reduced Nusselt number in the domain of $0 \le \xi \le 1$ when $\mathrm{Pr} = 10$, $Nt = Nb = 0.1$, Le = 10, and $S = 0.2$.

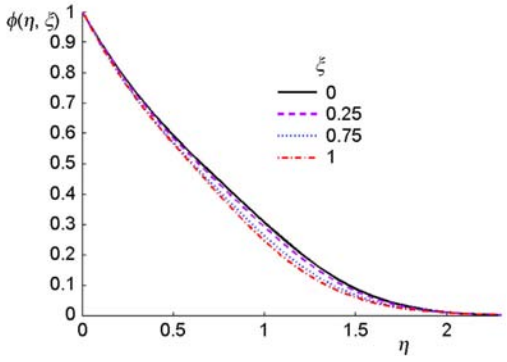

Figure 9. Variations in ϕ profiles for different ξ

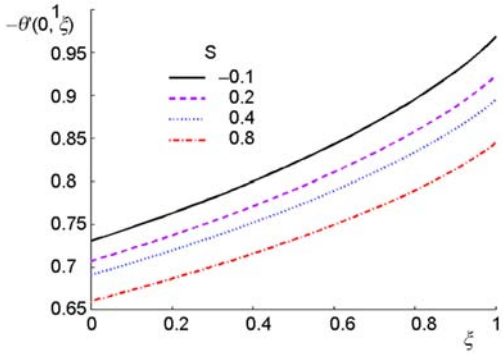

Figure 10. Variations in $-\theta'(0, \xi)$ with S and ξ

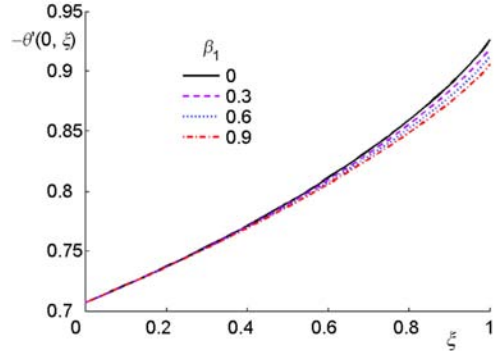

Figure 11. Variations in $-\theta'(0, \xi)$ with β_1

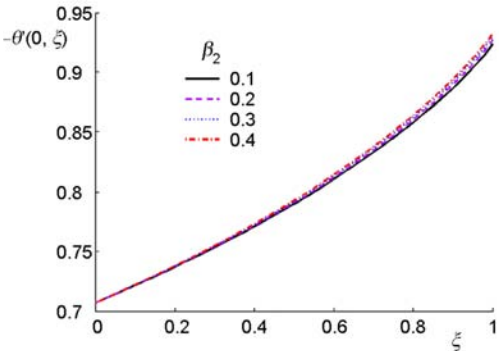

Figure 12. Variations in $-\theta'(0, \xi)$ for different β_2

Conclusions

Time dependent boundary layer flow of Oldroyd-B NF over an impulsively stretching plate has been investigated. Heat transfer analysis is carried out by taking thermal conductivity as a function of temperature. The numerical solutions for velocity, temperature and NP concentration were computed using a bivariate spectral collocation approach which was being applied for the first time on systems of coupled partial differential equations with fluid mechanics applications. The numerical method was found to give accurate results which converged rapidly. Other significant findings from this study are summarized as follows.

- Thermal boundary layer thickness increases with the increase of thermal conductivity parameter.
- Time has decreasing influence on the fluid temperature and nanoparticle concentration between initial unsteady state (*i. e.* $\xi = 0$), and final steady-state (*i. e.* $\xi = 1$).
- The effect of relaxation time is to decrease the rate of heat and mass transfer at the sheet. These effects become more pronounced as the flow reaches the steady-state.

- Increase in the magnitude of reduced Nusselt number is observed as we move from initial unsteady flow ($\xi = 0$) to the final steady-state flow ($\xi = 1$).
- Thermophoresis causes to increase the thickness of thermal boundary layer.

In view of the success of the bivariate spectral collocation method proposed in this work, the method can be recommended as a practical tool for solving similar non-linear PDE with applications in fluid mechanics.

Acknowledgment

This work is based on the research supported in part by the National Research Foundation of South Africa (Grant No: 85596)

Nomenclature

b – constant
c_p – effective heat capacity [$JK^{-1}m^{-3}$]
D_B – Brownian diffusion coefficient [$kgm^{-1}s^{-1}$]
D_T – thermophoresis diffusion coefficient [$kgm^{-1}s^{-1}K^{-1}$]
k – thermal conductivity [$WK^{-1}m^{-1}$]
K_1 – relaxation time [s]
K_2 – retardation time [s]
Le – Lewis number [–]
Nb – Brownian motion parameter [–]
Pr – Prandlt number [–]
Re_x – local Reynolds number [–]
S – thermal conductivity parameter [–]
T – temperature [K]
u, v – velocity components along x- and y-axis

Greek symbols

ν – kinematic viscosity [m^2s^{-1}]
ρ – mass density [kgm^{-3}]
τ – dimensionless time [–]

References

[1] Choi, S. U. S., *Enhancing Thermal Conductivity of Fluids with Nanoparticles, Developments and Applications of non-Newtonian Flows* (Eds. D. A. Siginer, H. P. Wang), FED-Vol. 231/MD-vol. 66, ASME, New York, USA, 1995, pp. 99-105
[2] Choi, S. U. S., *et al.*, Anomalously Thermal Conductivity Enhancement in Nanotube Suspensions, *Appl. Phys. Lett., 79* (2001), 14, pp. 2252-2254
[3] Buongiorno, J., Convective Transport in Nanofluids, *J. Heat Transfer, 128* (2006), 3, pp. 240-250
[4] Nadeem, S., *et al.*, Numerical Solution of non-Newtonian Nanofluid Flow over a Stretching Sheet, *Appl. Nanosci., 4* (2014), 5, pp. 625-631
[5] Nadeem, S., *et al.*, Numerical Study of Boundary Layer Flow and Heat Transfer of Oldroyd-B Nanofluid towards a Stretching Sheet, *PLoS ONE, 8* (2013), 8, e69811
[6] Uddin, M. J., *et al.*, Group Analysis and Numerical Computation of Magneto-Convective non-Newtonian Nanofluid Slip Flow from a Permeable Stretching Sheet, *Appl. Nanosci., 4* (2014), 7, pp. 897-910
[7] Khan, W. A., *et al.*, Three Dimensional Flow of an Oldroyd-B Nanofluid Towards Stretching Surface with Heat Generation/Absorption, *PLoS ONE, 9* (2014), 8, e105107
[8] Bachok, N., *et al.*, Unsteady Boundary Layer Flow and Heat Transfer of a Nanofluid over a Permeable Stretching/Shrinking Sheet, *Int. J. Heat Mass Transf., 55* (2012), 7, pp. 2102-2109
[9] Khan, M. S., *et al.*, Unsteady MHD Free Convection Boundary Layer Flow of a Nanofluid along a Stretching Sheet with Thermal Radiation and Viscous Dissipation Effects, *Int. Nano Letters, 2* (2012), 24, pp. 1-24
[10] Mustafa, M., *et al.*, Unsteady Boundary Layer Flow of Nanofluid past an Impulsively Stretching Sheet, *J. Mechanics, 29* (2013), 3, pp. 423-432
[11] Beg, O. A., *et al.*, Explicit Numerical Study of Unsteady Hydromagnetic Mixed Convective Nanofluid Flow from an Exponentially Stretching Sheet in Porous Media, *Appl. Nanosci., 4* (2014), 8, pp. 943-957
[12] Bhatnagar, R. K., *et al.*, Flow of an Oldroyd-B Fluid due to a Stretching Sheet in the Presence of a Free Stream Velocity, *Int. J. Non-Linear Mech., 30* (1995), 3, pp. 391-405
[13] Hayat, T., *et al.*, Some Simple Flows of an Oldroyd-B Fluid, *Int. J. Eng. Sci., 39* (2001), 2, pp. 135-147
[14] Sajid, M., *et al.*, Boundary Layer Flow of an Oldroyd-B Fluid in the Region of Stagnation Point over a Stretching Sheet, *Can. J. Phys., 88* (2010), 9, pp. 635-640

[15] Hayat, T., *et al.*, Three Dimensional Flow of Oldroyd-B Fluid over Surface with Convective Boundary Condition, *Appl. Math. Mech., 34* (2013), 4, pp. 489-500
[16] Shehzad, S. A., *et al.*, Three Dimensional Flow of an Oldroyd-B fluid with Variable Thermal Conductivity and Heat Generation/Absorption, *PLoS ONE, 8* (2013), 11, e78240
[17] Motsa, S. S., *et al.*, A Bivariate Chebyshev Spectral Collocation Quasilinearization Method for Nonlinear Evolution Parabolic Equations, *The Scientific World Journal, 2014* (2014), ID 581987
[18] Trefethen, L. N., *Spectral Methods in MATLAB*, SIAM, Philadelphia, Penn., USA, 2000

Paper submitted: October 10, 2014
Paper revised: January 1, 2015
Paper accepted: February 2, 2015